Supplementary Material 1 – supplementary text

1. Coastal settings

The approach is applied to the open ocean beaches of the French Aquitaine coast (Bay of Biscay). This sandy coast is 230 km long, sparsely urbanized, and constituted by high-energy meso-macrotidal open beaches which are backed by high (generally 15 to 20 m) and wide (generally larger than 100 m) coastal dunes. Topographic transects of the beach-dune systems are annually monitored with cm-level precision surveys using differential kinematic Global Positioning System (GPS) since 2008 over more than 20 transects (Bulteau et al., 2014), providing useful data to analyze inter-annual variations of the beach-dune system (dune nourishment by aeolian processes, slopes of the upper shoreface). Furthermore, an analysis of past shoreline positions based on remote sensing images allows to analyze shoreline variability and trends at different timescales (Supplementary Material 4; Castelle et al., 2018). Panels B and C in Supplementary Material 4 show that the estimation of multi-decadal trends and variability of shoreline positions are mostly insensitive to the removal of the least reliable shoreline position (1950), suggesting that the evaluation of shoreline change variability and trends are robust against outliers and missing shoreline data. Hence, owing to these observations, a probability distribution can be proposed to represent the uncertainties of the different processes contributing to shoreline changes included in equation (1) (Supplementary Material 2). Four contrasted sites are selected to perform reconstructions and projections of shoreline positions and to analyze the uncertainties (Supplementary Material 2, 3 and 4).

2. Method used to generate virtual time series of events

The PCR model requires simulating virtual time series of the following statistically dependent variables: significant wave height Hs, peak period Tp, peak direction θp, event duration D, surge η, tidal level A, spacing between events G. We used wave data from BoBWA_10kH database (Charles et al., 2012 ; http://bobwa.brgm.fr). The extracted point is located (44.65°N ; -1.45°E) at 51 m depth and the covered period is 1958-2002 at hourly time step. Surges and tidal signal come from a reanalysis covering the

period 1979-2009 at 10 min time step (Paris et al., 2013). The full temporal simulation proceeds in seven steps:

1- Select independent events from original time series of waves and surge. Following the approach of Gouldby et al. (2014) we introduced a notional flooding level based on wave setup calculated with the formula of Stockdon et al. (2006) and surges:

$$FL = setup + \eta$$

A flooding level time series of 23.66 years is thus created. Independent events are then selected using a Peaks-Over-Threshold (POT) approach and appropriate independence temporal criteria (minimum of 1 day between the end of an event and the beginning of the next one, or, if it is not verified, a minimum of 2 days between two consecutive FL peaks). We end up with 473 independent combinations of (Hs, Tp, θp, D, η).

2- Fit extreme value distributions (Generalized Pareto Distributions) to wave height Hs, surge η and storm duration D (marginal distributions).

3- Fit the semi-parametric conditional extreme model of Heffernan and Tawn (2004) to model dependencies between Hs, D and η.

4- Fit a non-homogenous Poisson distribution to the spacing between storms G taking into account event grouping as in Callaghan et al. (2008) and Luceño et al. (2006).

5- Generate times series of combinations of (Hs, D, η, G) representing 100 years by means of a Monte-Carlo procedure.

6- Fit the peak wave period and peak direction conditional distributions (conditioned to Hs) and complete the synthetic dataset with simulations of Tp and θp. The same models as in Gouldby et al. (2014) are used for Tp and θp.

7- Finally, simulate the tidal level A for each synthetic event. To do so, a Saros period (18.6 years) of the tidal signal is duplicated multiple times so that the total length covers the simulated period (100 years). Then, we select the tidal peak closest to each simulated event.

Steps 5 to 7 are repeated multiple times to be able to characterize the uncertainty due to random Monte Carlo simulations.

3. Surrogate of the PCR model

The gray areas in the Figure provided in Supplementary Material 5 show the variability of the PCR model response due to its response to 50 time series of virtual events (see Methods). Dark gray indicates likely shoreline change rates, whose probability is larger than 66% according to the simulations (consistently with the IPCC language on uncertainties). Light gray areas provide information regarding higher quantiles, displaying the possible values of very likely and virtually certain shoreline change rates according to the PCR simulations. The standard deviation of the shoreline positions obtained with the PCR model is less than 9 m given a fixed sea level rise step, which is smaller or of the same order than the observed shoreline change variability (8 to 20 m according to the panel B in the Figure of Supplementary Material 4). This shoreline change variability is included in equation (1) through the term $Lvar$.

Supplementary Material 5 shows that in a first approximation, the equilibrium response of the PCR model can be emulated by equation (2), where the slopes of the upper shoreface (from 4 to 13%, see Supplementary Material 2) are substituted to the Bruun slopes (from 1.2 to 1.5% in Aquitaine). Finally, using equation (1) with the Bruun rule or the PCR surrogate model has a negligible computation time, so that it becomes possible to perform a propagation of probabilistic uncertainties and a global sensitivity analysis by means of a quasi-Monte-Carlo procedure.

4. References of the supplementary material:

1. Bernon N., Mallet C., Belon, R., Hoareau A., Bulteau T. et Garnier C. (2016), caractérisation de l'aléa recul du trait de côte sur le littoral de la côte aquitaine aux horizons 2025 et 2050. Rapport final. BRGM/RP-66277-FR, 99p., 48 ill., 16 tab., 2 ann. http://infoterre.brgm.fr/rapports/RP-66277-FR.pdf
2. Bulteau T., Mugica J., Mallet C., Garnier C., Rosebery D., Maugard F., Nicolae Lerma A., Nahon A. avec la collaboration de Millescamps B. (2014) – Évaluation de l'impact des tempêtes de l'hiver 2013- 2014 sur la morphologie de la Côte Aquitaine. Rapport final.

BRGM/RP-63797-FR, 68 p., 138 fig., 8 tab., 2 ann.
http://www.brgm.fr/sites/default/brgm/projets/oca/RP-63797-FR.pdf

3. Callaghan D, Nielsen P, Short A, Ranasinghe R (2008) Statistical simulation of wave climate and extreme beach erosion. Coast Eng 55(5):375–390

4. Gouldby, B., Méndez, F. J., Guanche, Y., Rueda, A., and Mínguez, R.: A methodology for deriving extreme nearshore sea conditions for structural design and flood risk analysis, Coast. Eng., 88, 15–26, 2014.

5. Heffernan, J. E. and Tawn, J. A. «A conditional approach for multivariate extreme values.» *Journal of the Royal Statistical Society*, 2004: 66, 3, 497-546.

6. Idier, D., Castelle, B., Charles, E., & Mallet, C. (2013). Longshore sediment flux hindcast: spatio-temporal variability along the SW Atlantic coast of France. *Journal of Coastal Research*, *65*(sp2), 1785-1790.

7. Luceño, A., Menéndez, M., Méndez, F., 2006. The effect of temporal dependence on the estimation of the frequency of extreme ocean climate events. Proceedings of the Royal Society of London, Series A 462 (2070), 1683–1697.

1 **Supplementary Material 2 – supplementary Table**

2 Probabilistic representation of the uncertainties of input parameters in equation (1).

Variable	Distribution	Values	Source of information
Beach slope from the dune toe to the depth of closure	Uniform	1.2% to 1.5%	Yearly beach profile surveys (DGPS) of the Aquitaine Coastal Observatory (Bernon et al., 2016)
Slope of the upper shoreface (Larson et al., 2004)	Uniform	Site #1 (km 55) : 4% to 10% Site #2 (km 140) : 6% to 12% Site #3 (km 165) : 6% to 13% Site #4 (km 197) : 5% to 13%	Yearly beach profile surveys (DGPS) of the Aquitaine Coastal Observatory (Bulteau et al., 2014)
Coastal impact model	Discrete uniform	Bruun or emulation of Ranasinghe	Bruun (1962) Ranasinghe et al. (2012)
Variability of shoreline position at timescales ranging from events to several decades	Gaussian	Site 1 (km 55) : +/-3.2m Site 2 (km 140) : +/- 9.4m Site 3 (km 165) : +/-21m Site 4 (km 197) : +/-8.5m	Based on past observed multi-decadal shoreline change variability (Castelle et al., 2018; see Supplementary Material 4).
Linear trend of shoreline evolution at longer timescales	Gaussian	Site 1 : 0.15+/-0.12m/yr Site 2 : -0.083+/-0.22m/yr Site 3 : 1.08+/-0.28m/yr Site 4 : 0.82+/-0.11m/yr	Based on past observed multi-decadal shoreline change variability (Castelle et al., 2018; see Supplementary Material 4).
Vertical ground motion	Gaussian	Site 1 : 0+/-2mm/yr Site 2 : -1,2±0,6 mm/yr (GNSS) Site 3 : 0+/-2mm/yr Site 4 : 0+/-2mm/yr	Based on the permanent GNSS located at Cap-Ferret (site #2). For the other sites, no trend can be computed yet (short records), and the uncertainties of vertical ground motion is based on the mean and standard deviation of all permanent GNSS velocities in the SONEL database (Santamaria-Gomez et al., 2017) after removal of the effects of the global isostatic adjustment using the ICE-5G model (Peltier, 2004) (see Methods).
Past regional sea level rise	Gaussian	Sea Figure 1	Based on a reconstruction of past sea level in the Bay of Biscay (see Methods)
Future regional sea level rise	Non parametric distribution	See Figure 1	Data of La Rochelle (Kopp et al., 2014), corrected from vertical ground motions measured with a permanent GNSS station (see methods)
Climate change scenario	Discrete uniform	RCP 2.6, 4.5 or 8.5	Kopp et al., 2014; See Figure 1.

3

Supplementary Material 3 – supplementary Figure

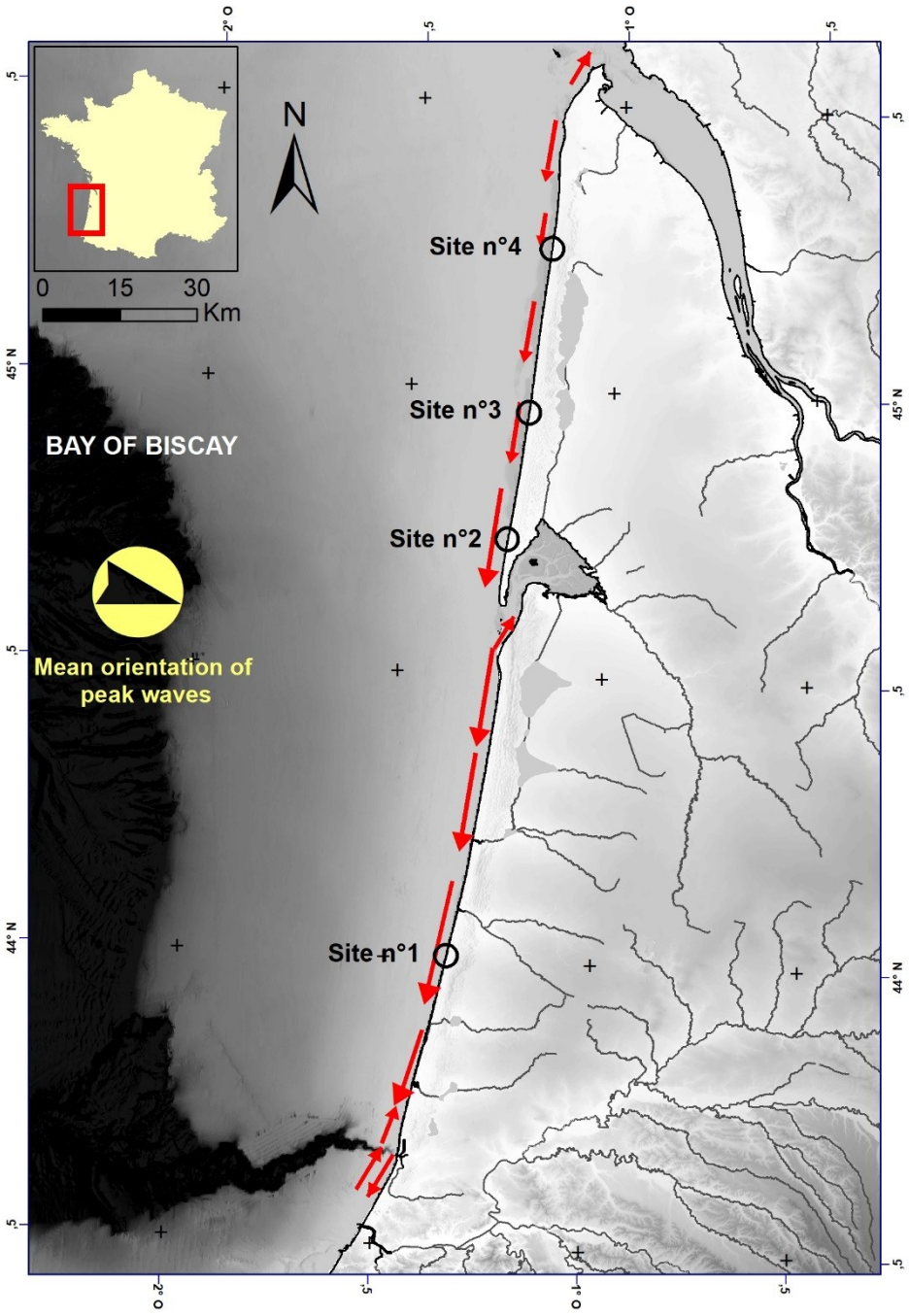

Map showing the location of four selected coastal sites in Aquitaine, the mean orientation of peak waves and the longshore sediment fluxes (adapted from Idier et al., 2013).

Supplementary Material 4 – supplementary Figure

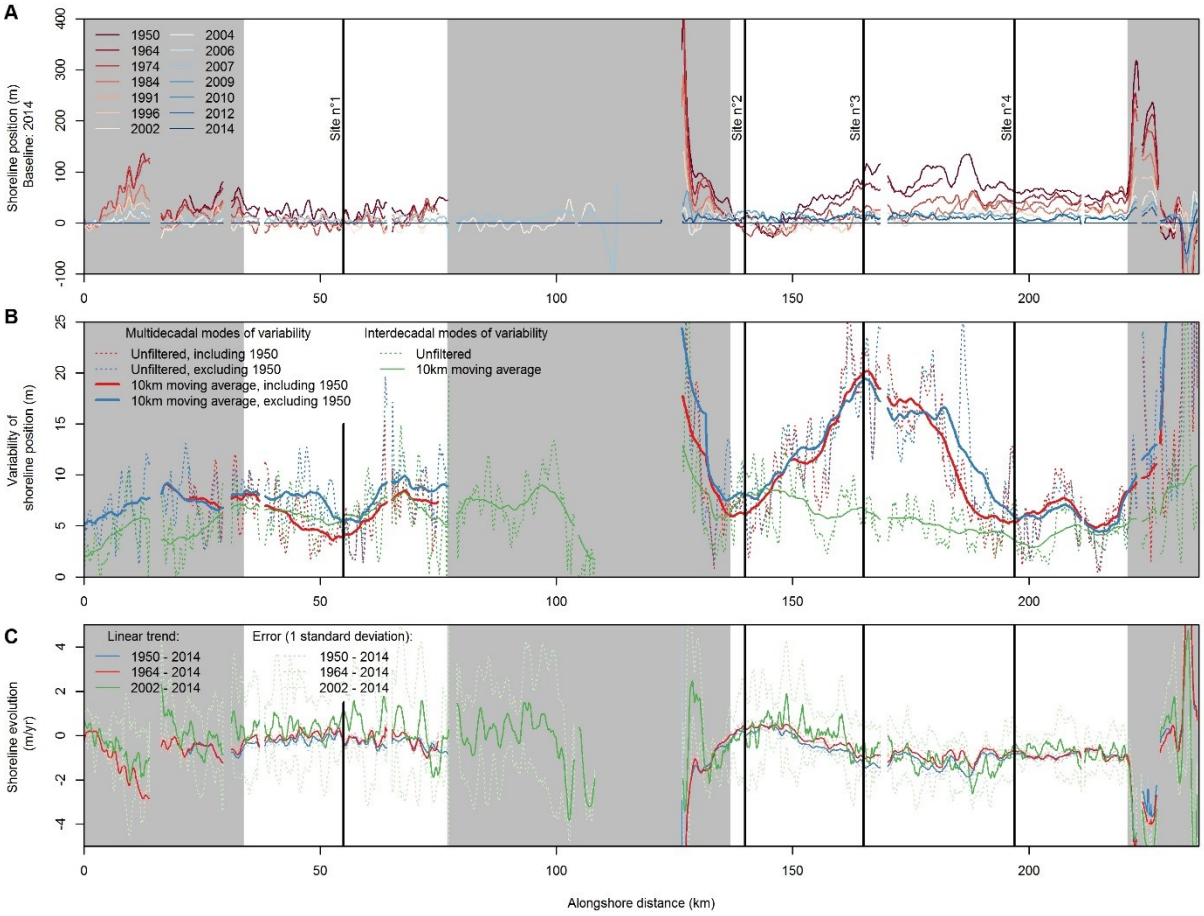

Spatial variability of shoreline position (A), shoreline change variability (B) and trends (C) along the sandy shorelines of Aquitaine. In Panel B, shoreline change variability is estimated as the standard deviation of the de-trended shoreline positions for each transect with at least 3 observations over 3 different decades (blue and red curves) and using all shoreline positions available from 2002 to 2014 (green curves). In areas unaffected by estuarine processes, the average shoreline change variability accounts for ±9.8m around the linear multi-decadal trend if all shorelines (including 1950) are included. The grey areas indicate coastal sites excluded from the analysis, either because they are too close from estuaries or because of the lack of shoreline data (Data: Castelle et al., 2018).

Supplementary Material 5– supplementary Figure

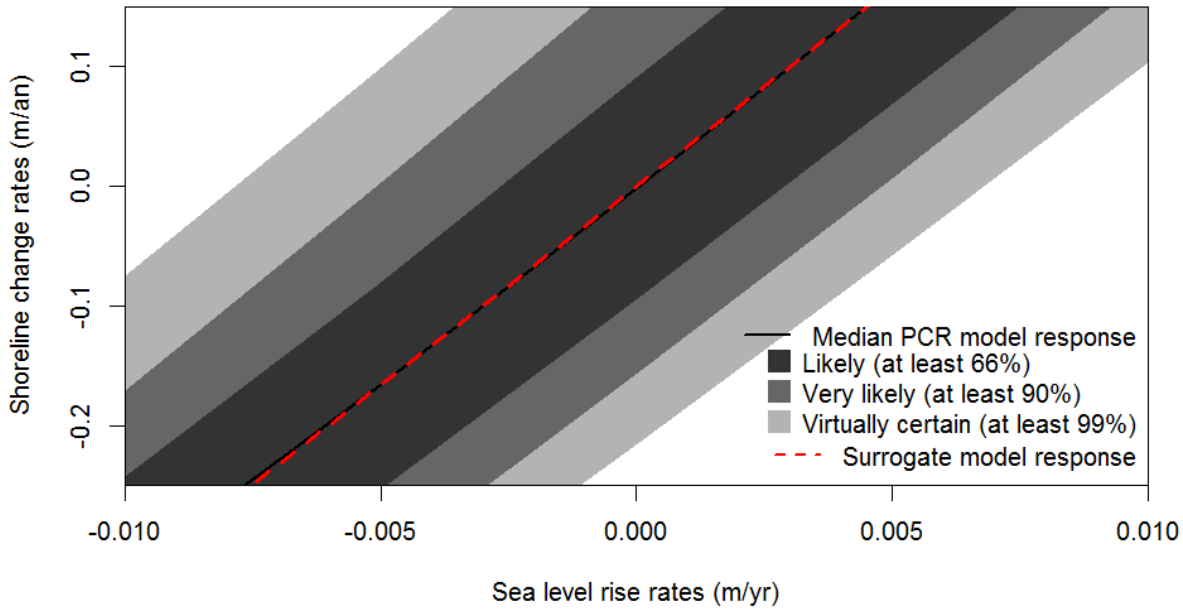

Shoreline change rates and related uncertainties for values of sea level rise ranging from -25mm/yr to +15mm/yr using the PCR model and its surrogate to site #2 (see Methods). Shoreline retreats are computed assuming that the shoreline is at equilibrium at the beginning of the simulations, and that the upper beach slope is equal to 3%. The uncertainties of shoreline change rates originate from the use of 50 random time series of 100 years of virtual events as well as from the nourishment of the dune between extreme events (see Supplementary Material 1).

Supplementary Material 6– supplementary Figure

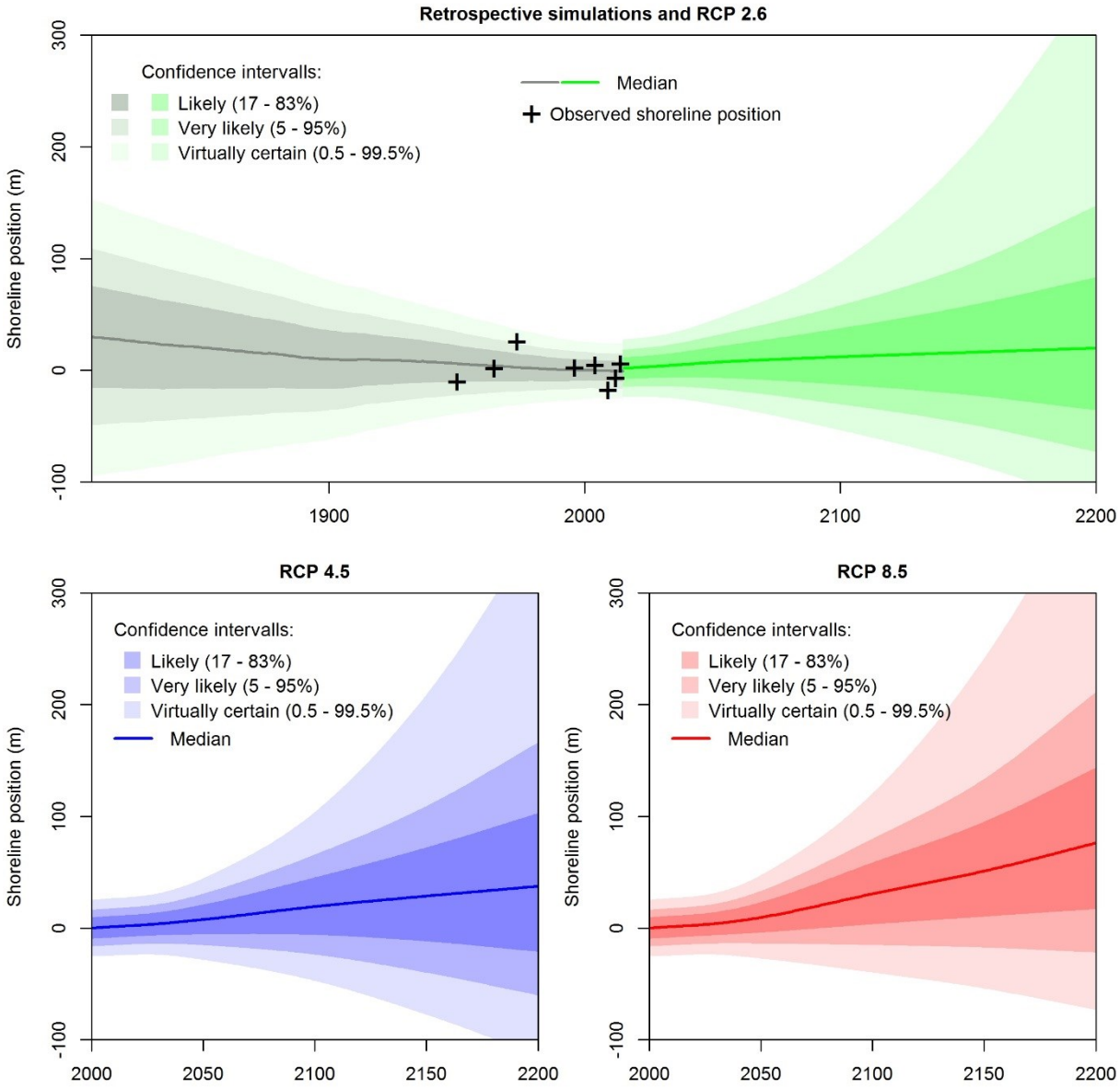

Same as Figure 2, for the site #2.

Supplementary Material 7– supplementary Figure

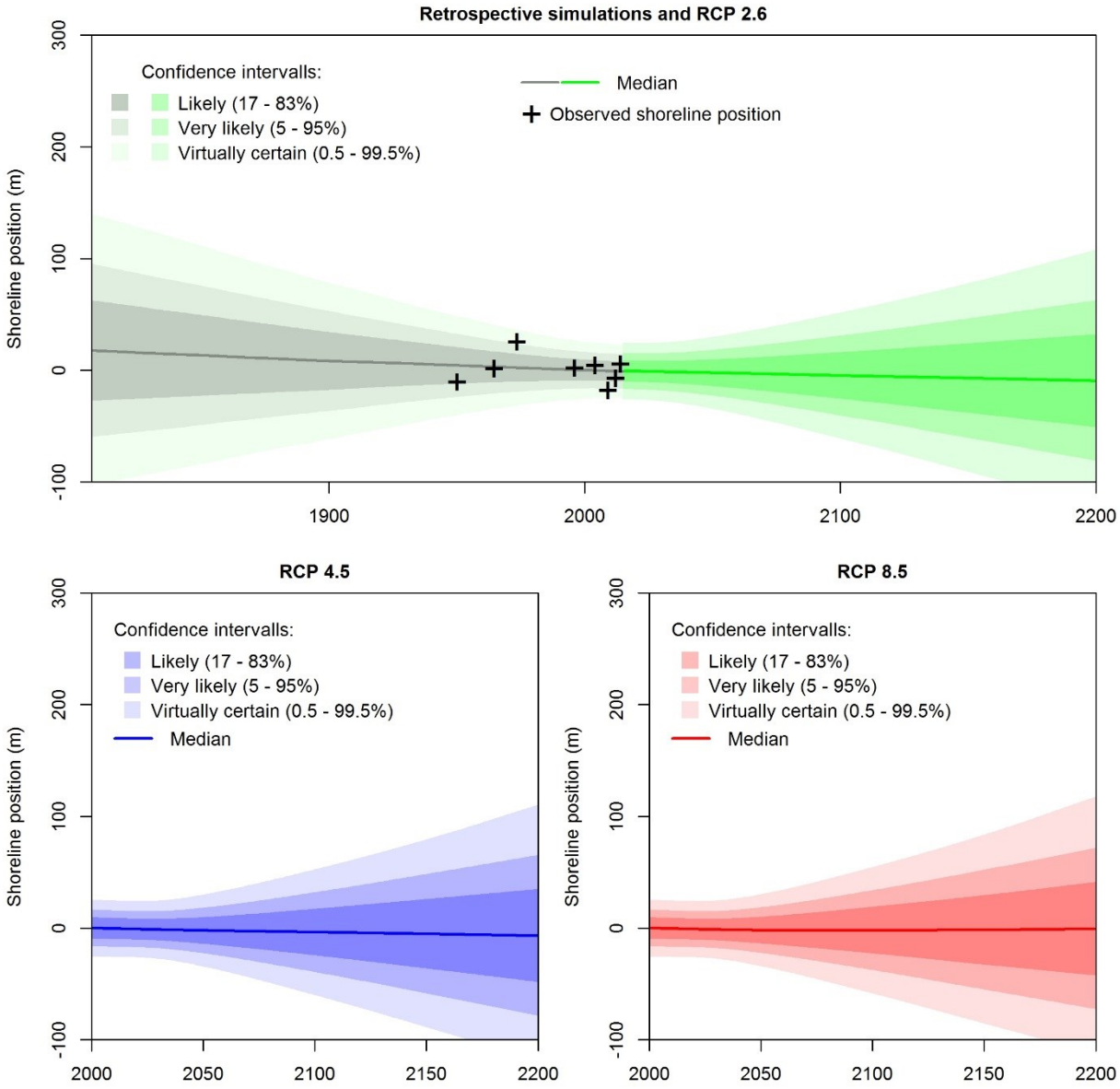

Same as Figure 3, for the site #2

Supplementary Material 8– supplementary Figure

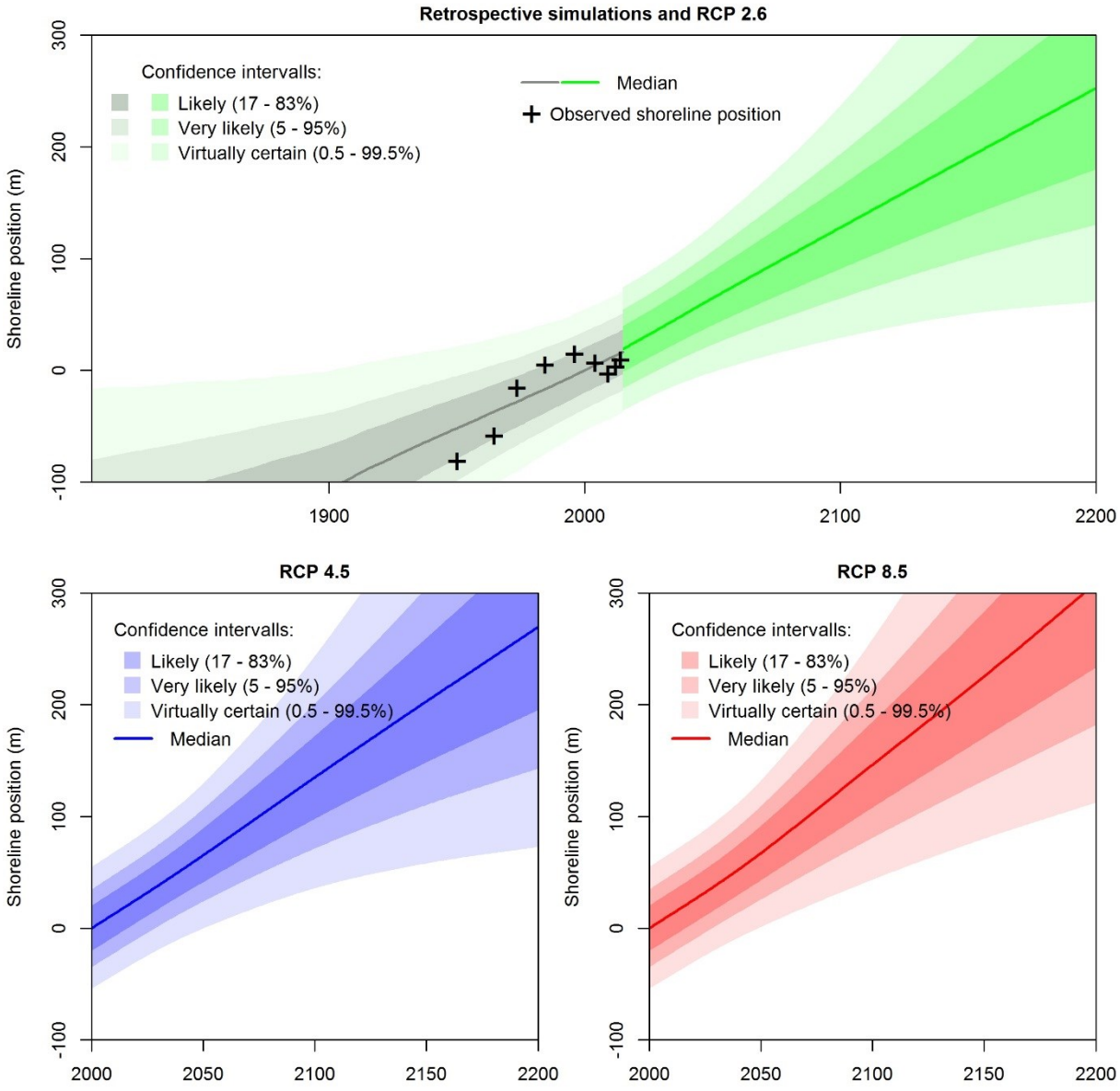

Same as Figure 2, for the site #3.

Supplementary Material 9– supplementary Figure

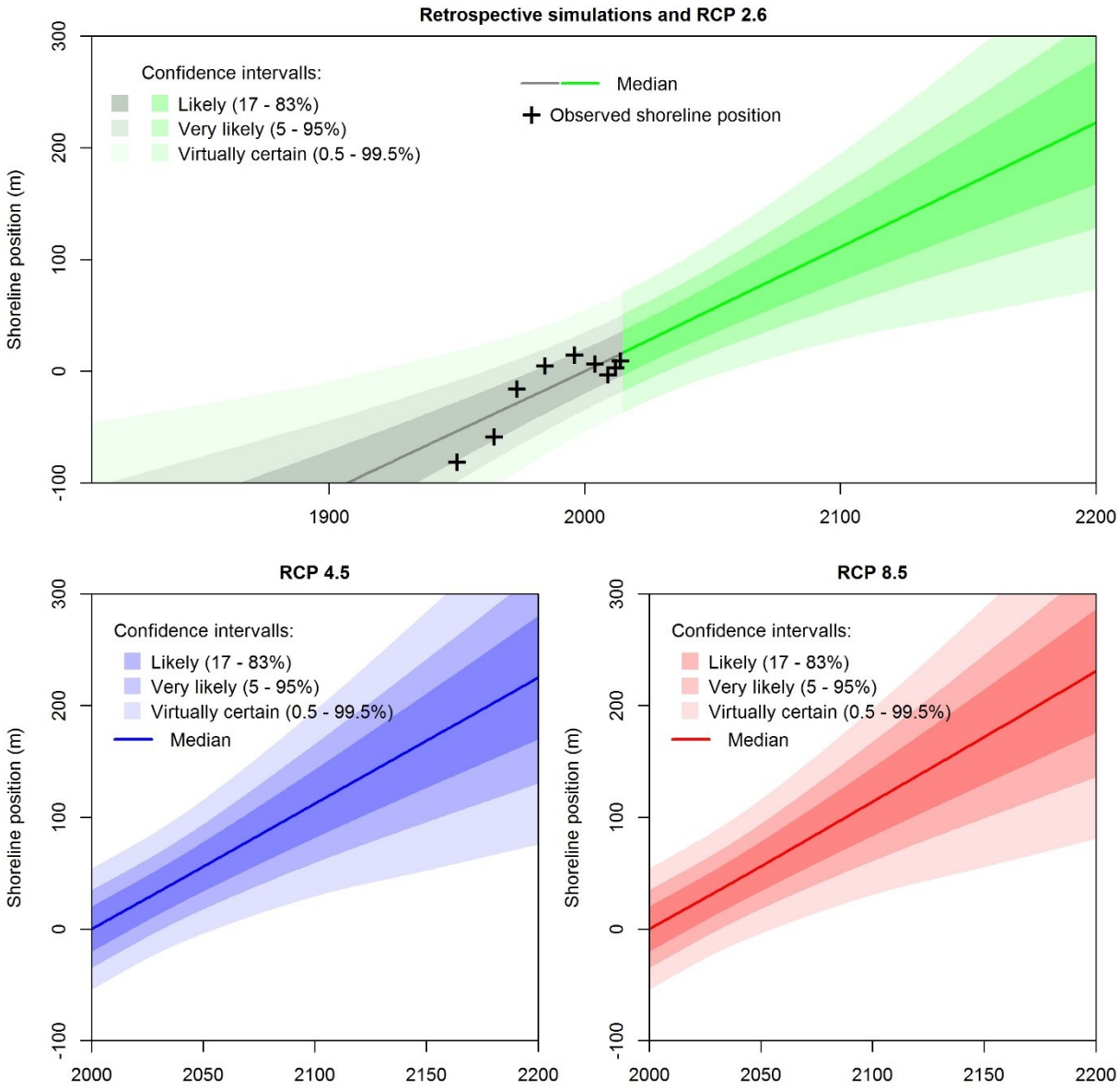

Same as Figure 3, for the site #3.

Supplementary Material 10– supplementary Figure

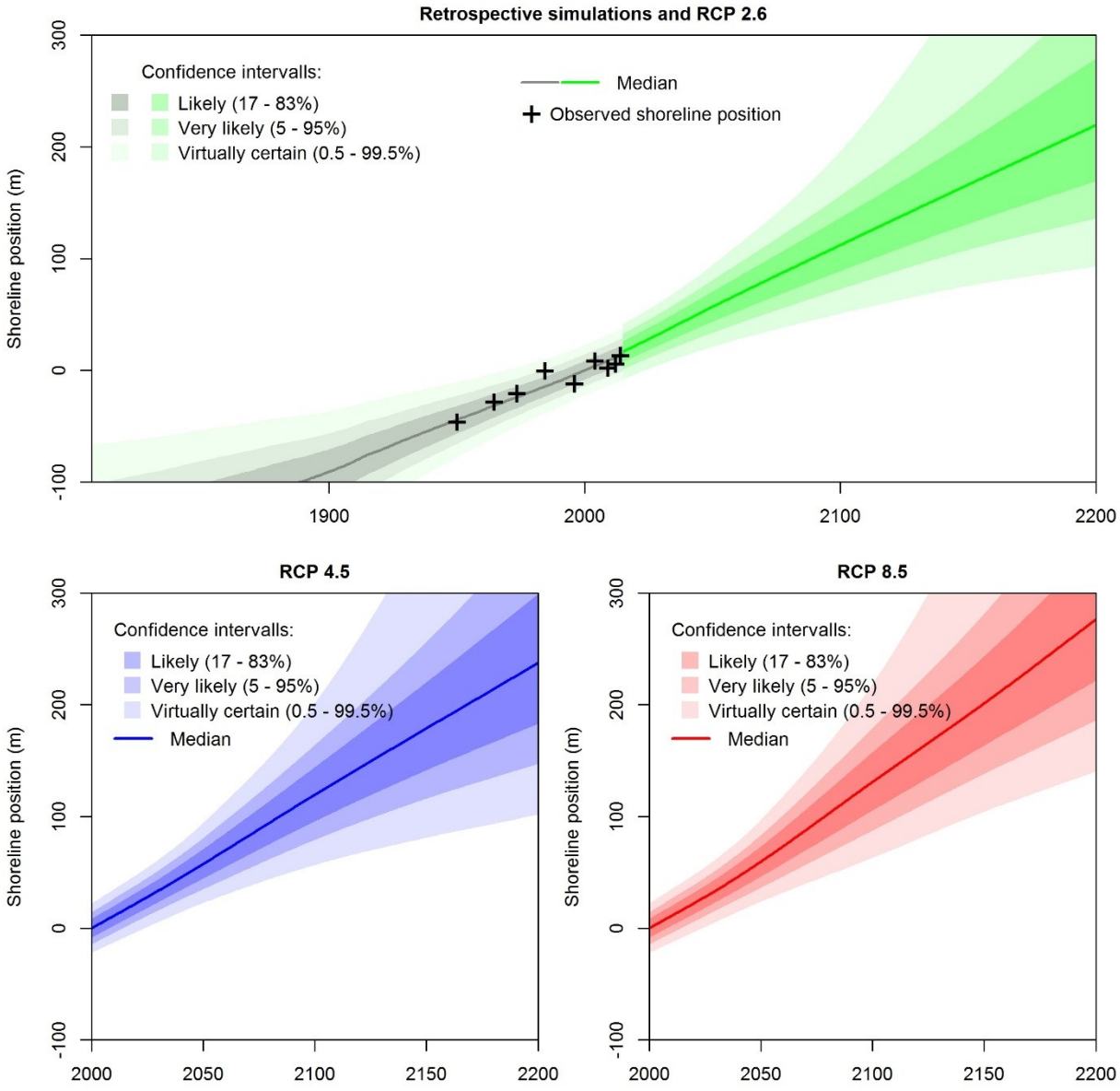

Same as Figure 2, for the site #4.

Supplementary Material 11– supplementary Figure

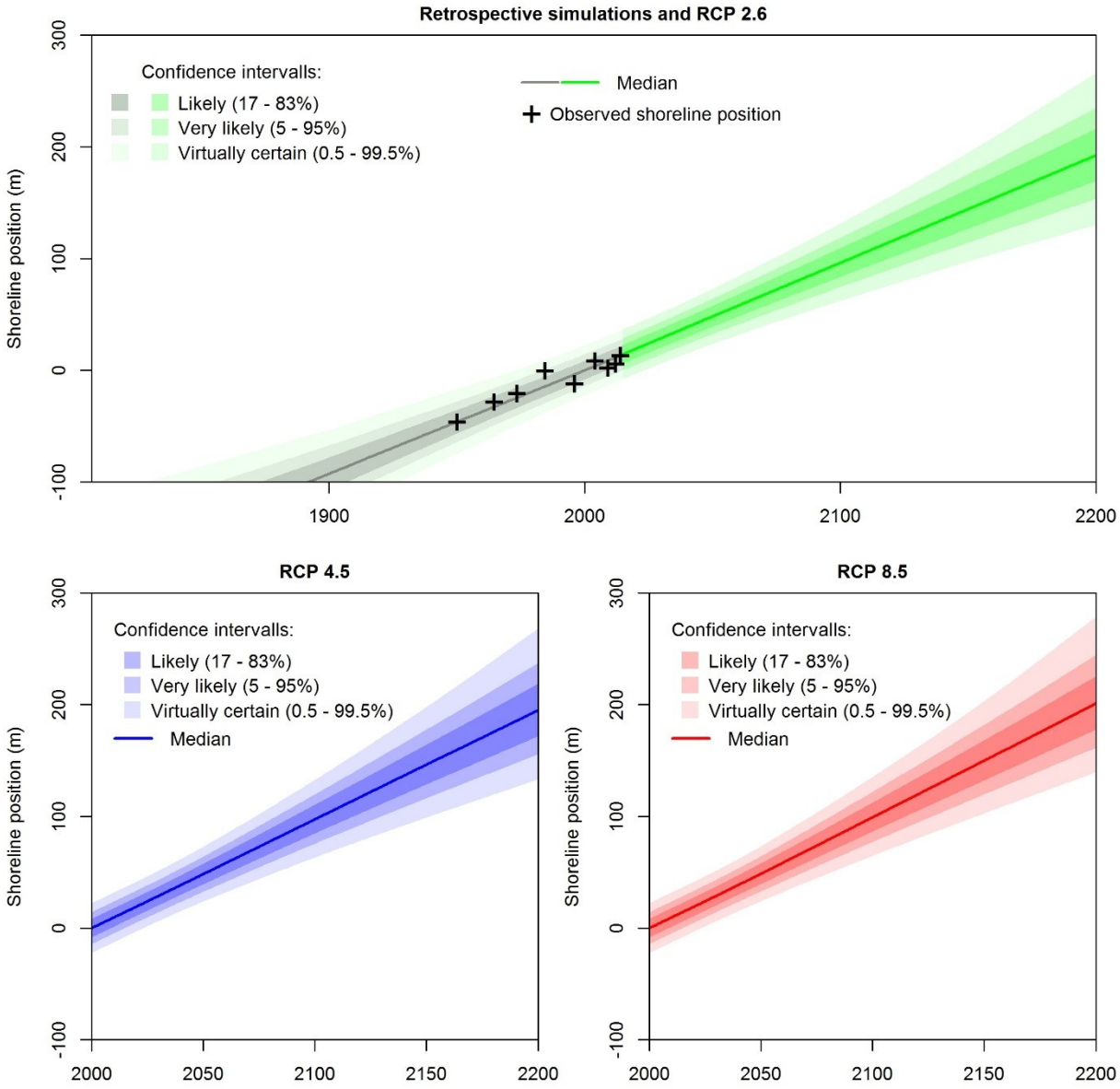

Same as Figure 3, for the site #4.